Soft Matter

Self-Assembly of Magnetic Colloids with Radially Shifted Dipoles

Journal:	*Soft Matter*
Manuscript ID	SM-ART-10-2019-002020.R2
Article Type:	Paper
Date Submitted by the Author:	11-Jan-2020
Complete List of Authors:	Victoria Camacho, Jonathan Alfredo; University of Puerto Rico Mayaguez, Bio-Engineering; DeLaCruz-Araujo, Ronal; University of Puerto Rico, Chemical Engineering Kretzschmar, Ilona; City College of the City University of New York, Chemical Engineering Córdova-Figueroa, Ubaldo; University of Puerto Rico, Mayagüez , Department of Chemical Engineering

SCHOLARONE™
Manuscripts

Journal Name

Self-Assembly of Magnetic Colloids with Radially Shifted Dipoles[†]

Jonathan A. Victoria-Camacho,[a] Ronal A. DeLaCruz-Araujo,[b] Ilona Kretzschmar[c] and Ubaldo M. Córdova-Figueroa[*b]

Anisotropic potentials in Janus colloids provide additional freedom to control particle aggregation into structures of different sizes and morphologies. In this work, we perform Brownian dynamics simulations of a dilute suspension of magnetic spherical Janus colloids with their magnetic dipole moments shifted radially towards the surface of the particle in order to gain valuable microstructural insight. Properties such as the mean cluster size, orientational ordering, and nucleation and growth are examined dynamically. Differences in the structure of clusters and in the aggregation process are observed depending on the dipolar shift (s)—the ratio between the displacement of the dipole and the particle radius—and the dipolar coupling constant (λ)—the ratio between the magnetic dipole-dipole and Brownian forces. Using these two dimensionless quantities, a structural "phase" diagram is constructed. Each phase corresponds to unique nucleation and growth behavior and orientational ordering of dipoles inside clusters. At small λ, the particles aggregate and disaggregate resulting in short-lived clusters at small s, while at high s the particles aggregate in permanent triplets (long-lived clusters). At high λ, the critical nuclei formed during the nucleation process are triplets and quadruplets with unique orientational ordering. These small clusters are then serving as building blocks to form larger structures, such as single-chain, loop-like, island-like, worm-like, and antiparallel-double-chain clusters. This study shows that dipolar shifts in colloids can serve as a control parameter in applications where unique size, morphology, and aggregation kinetics of clusters are required.

1 Introduction

Magnetic colloids are becoming increasingly important in materials science, owing by the ability to manipulate their structures formed through varying magnetic interactions. Either natural[1,2] or synthetic,[3] they have a great value for several biomedical applications, such as tumor treatment, drug delivery, resonance imaging, tissue engineering, and environmental remediation.[4–7]

Also, in recent years, the works on magnetic Janus particles (where the magnetic dipole is displaced from the particle center) have show additional freedom to control particle aggregation into clusters of different sizes and morphologies not observed

with typical magnetic colloids (with centered magnetic dipole moment).[8–11] These new aggregation behaviors are caused by the additional interaction anisotropy due to the shift of the magnetic dipole out of the particle center, showing new structures beyond chains, rings, and bundles.[12] To effectively use these new kinds of colloids, it is important to understand their dynamic aggregation processes.

In simulations and theoretical calculations, magnetic colloids are typically modeled as dipolar hard spheres (DHS). The DHS model consists of a rigid sphere with a constant diameter and a centered dipole moment.[13–15] By making adjustments to the DHS model, we can invoke anisotropy by shifting of the magnetic dipole, i.e., a magnetic dipole that is off-centered with an angle between the direction of the displacement and the magnetic dipole moment. When the dipole displacement is orthogonal to the surface of the particle, this is referred to as "radially shifted", since the displacement occurs in the same direction as the dipole moment. On the other hand, the magnetic dipole can also be shifted laterally and have other configurations.[16–18]

Magnetic particles with radially shifted dipoles have been fabricated experimentally by evaporation of Co/Pt on top of silica

[a] *Department of Mechanical Engineering, University of Puerto Rico–Mayagüez, Mayagüez, PR 00681, USA.*

[b] *Department of Chemical Engineering, University of Puerto Rico–Mayagüez, Mayagüez, PR 00681, USA. E-mail: ubaldom.cordova@upr.edu*

[c] *Department of Chemical Engineering, City College of New York, City University of New York, NY 10031, USA.*

particles.[19] Here, the out-of-plane magnetic anisotropy causes radially shifted dipoles, which results in the formation of island-like structures for certain dipole shifts proving the accessibility of this magnetic "Janus" colloid through synthesis and opening the question of what happens at other dipole shifts. The radial shift is expected to induce the formation of unique colloidal clusters with their own structure and dynamics, as similarly demonstrated for magnetic colloids with lateral shifts of the magnetic dipole.[18]

Previously, the structures of Janus particles with radially shifted dipoles have been studied mostly focusing on the equilibrium properties of the system by Monte Carlo simulations.[20,21] These results have shown the dependence of particle orientations on the shift in the ground state corresponding to the minimum energy. However, in order to utilize these colloidal systems in applications, it is important to understand their self-assembly process. To do so, we need to know the rate of aggregation and the stages of nucleation and growth to compare with other systems and identify dynamic building blocks and long-term behaviors to compare this system with classical power laws.

We have conducted Brownian dynamics simulations[22–24] to analyze aggregation and dynamic structures in a quasi-two-dimensional (q2D) suspension of magnetic Janus colloids with radially shifted dipoles. We observe how dynamic aggregation affects the growth of clusters. The colloids are assembled in building blocks with relative orientations between them based on their minimum energy configuration, and by cluster-cluster aggregation they form larger structures whose morphology depends on the direction of movement of the building blocks.

This work is organized as follow: In the Problem formulation section, we introduce the model and discuss the governing equations for the system, i.e., the magnetic interactions between two radially shifted dipole particles to understand the behavior of the particle-particle interaction. In the Results section, we discuss the simulation results in a way to construct a structural "phase" diagram based on the dynamic cluster nucleation and growth and the orientation distributions. Finally, in the Conclusions section the main findings are summarized.

2 Problem Formulation

2.1 Model

Using the DHS model with the off-centered dipole moment and considering identical ferromagnetic colloidal particles with a permanent dipole, the radius a and the absolute radial shift of the dipole S can be related to the dipolar shift s. Here, the dipolar shift s denotes the relation between the absolute shift and the particle radius, i.e., $s = S/a$, where s ranges from 0 (particle center) to 1 (at the surface).

Fig. 1 shows the model system with the inertial frame of reference (x, y, z) fixed to the simulation box. In addition, each particle has its own mobile reference frame (x', y', z'). Values of position and orientation of each particle are initialized randomly. Hydrodynamic interactions are not considered in this model. The surface fraction ϕ_s was chosen to perform the simulation in the dilute limit, the parameters $\mathbf{m}_i$ and $\mathbf{m}_j$ denote the magnetic dipole moments of particles i and j, respectively. The q2D system is rep-

resentative of an experimental approach with the particles being assembled between two glass slides (the distance between the glass slides—at least 100 particle diameters—is neither a parameter that affects the aggregation mechanisms nor the structural properties of the systems).[25,26]
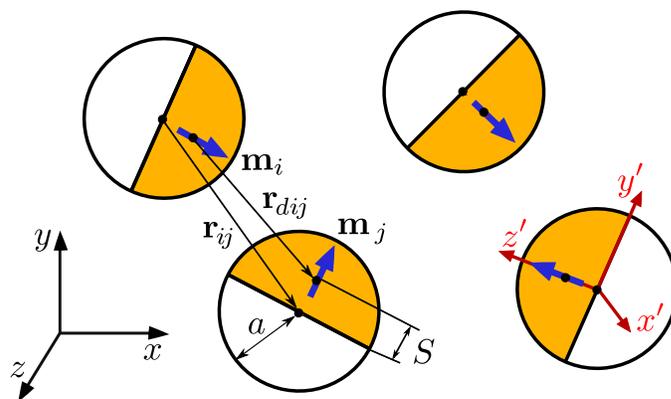

Fig. 1 Model system. The orange region represents the magnetic part of the colloids with a magnetic dipole moment ($\mathbf{m}_i$ or $\mathbf{m}_j$) radially displaced from the particle's center of mass by a distance S. Also, the reference (x, y, z) of the simulation box and the mobile reference to the colloid (x', y', z') are used to describe the dynamic position and orientation of the colloid.

2.2 Brownian Dynamics (BD) Simulation

The Brownian dynamics (BD) simulation considers three kinds of interactions; the first is given by Brownian motion as a result of thermal fluctuations by the surrounding Newtonian fluid, the second is given by the hydrodynamic drag, and the third is the particle-particle interaction. Inertia is negligible in our simulations as the movement is considered instantaneous at the colloidal scale. For a description of such a system, the translational and rotational overdamped Langevin equations are employed:[27]

$$\mathbf{F}^B + \mathbf{F}^D + \mathbf{F}^P = 0, \tag{1}$$

$$\mathbf{T}^B + \mathbf{T}^D + \mathbf{T}^P = 0, \tag{2}$$

where $\mathbf{F}^B$ and $\mathbf{T}^B$ are the Brownian force and torque, $\mathbf{F}^D$ and $\mathbf{T}^D$ are the drag force and torque and $\mathbf{F}^P$ and $\mathbf{T}^P$ are the summations of the forces and torques, respectively, given by the particle-particle interactions. More specifically, the particle-particle interactions are captured by the surface potential and the magnetic potential. The magnetic potential is given by:[28]

$$\Phi(r_{d_{ij}}) = -\frac{\mu_0}{4\pi} \left[3 \frac{\left(\mathbf{m}_i \cdot \mathbf{r}_{d_{ij}}\right)\left(\mathbf{m}_j \cdot \mathbf{r}_{d_{ij}}\right)}{r_{d_{ij}}^5} - \frac{\mathbf{m}_i \cdot \mathbf{m}_j}{r_{d_{ij}}^3} \right], \tag{3}$$

$$\mathbf{r}_{d_{ij}} = \mathbf{r}_{d_i} - \mathbf{r}_{d_j}, \quad r_{d_{ij}} = |\mathbf{r}_{d_{ij}}|,$$

where μ_0 is the vacuum permeability ($4\pi \cdot 10^{-7} H/m$), and $r_{d_{ij}}$ is the dipole-dipole distance. The surface potential only generates a force that acts in a steric region of thickness δ around the spherical colloid. The surface potentials are given by the steric repulsion force:[29,30]

$$F_{ij}^R = \begin{cases} kT\lambda_R \frac{1}{\delta} \ln\left(\frac{2(a+\delta)}{r_{ij}}\right) \mathbf{t}_{d_{ij}} & \text{if } 2a \leq r_{ij} \leq 2(a+\delta) \\ 0 & \text{if else} \end{cases}, \quad (4)$$

$$\mathbf{r}_{ij} = \mathbf{r}_i - \mathbf{r}_j, \quad r_{ij} = |\mathbf{r}_{ij}|, \quad \mathbf{t}_{d_{ij}} = \frac{\mathbf{r}_{ij}}{r_{ij}},$$

where k is the Boltzmann's constant $(1.3806488(13) \times 10^{23} J/K)$, T is the absolute temperature of the fluid, λ_R is the steric layer factor, and r_{ij} is the distance between the center of mass of the particles. Finally, the particle-particle force and torque are described by the following equations:

$$\mathbf{F}_{ij}^P = -\nabla\left(\mathbf{m}_i \cdot \mathbf{B}_{ij}\right) + F_{ij}^R, \quad (5)$$

$$\mathbf{T}_{ij}^P = \mathbf{m}_i \times \mathbf{B}_{ij} + \mathbf{s}_i \times \left[-\nabla\left(\mathbf{m}_i \cdot \mathbf{B}_{ij}\right)\right], \quad (6)$$

$$\Phi_{dd}(r_{d_{ij}}) = \mathbf{m}_i \cdot \mathbf{B}_{ij} \quad ; \quad \mathbf{s}_i = s\frac{\mathbf{m}_i}{|\mathbf{m}_i|}, $$

where $\mathbf{B}_{ij}$ is the magnetic field generated for the dipole $\mathbf{m}_j$ that interacts with the dipole $\mathbf{m}_i$.

The position and rotation of the particles are obtained upon integration of the Langevin equations (1) and (2). Integration with a finite differences approach yields the following results in dimensionless form:

$$\tilde{\mathbf{r}}_i(\tilde{t}+\Delta\tilde{t}) = \tilde{\mathbf{r}}_i(\tilde{t}) + \sum_{j=1\neq i}^{N}\left(\mathbf{I}\cdot\tilde{\mathbf{F}}_{ij}^P(\tilde{t})\right)\Delta\tilde{t} + \Delta\tilde{\mathbf{r}}_i^B(\tilde{t}), \quad (7)$$

$$\tilde{\mathbf{\Omega}}_i(\tilde{t}+\Delta\tilde{t}) = \tilde{\mathbf{\Omega}}_i(\tilde{t}) + \sum_{j=1\neq i}^{N}\left(\mathbf{I}\cdot\tilde{\mathbf{T}}_{ij}^P(\tilde{t})\right)\Delta\tilde{t} + \Delta\tilde{\mathbf{\Omega}}_i^B(\tilde{t}), \quad (8)$$

where $\mathbf{I}$ is the identity tensor, and $\Delta\tilde{\mathbf{r}}^B$ and $\Delta\tilde{\mathbf{\Omega}}^B$ are the dimensionless Brownian displacement and rotation contributions, respectively. In this equations the time was scaled with the characteristic diffusion time ($t \sim \tau_D$), the lengths were scaled with particle radius ($r \sim a$), forces with the Brownian force ($\mathbf{F} \sim kT/a$) and torques with the Brownian torque ($\mathbf{T} \sim kT$). The Brownian displacement and rotation contributions in equations (7) and (8) are related to the diffusion tensors as follows:

$$\left\langle\Delta\tilde{\mathbf{r}}_i^B\right\rangle = 0, \quad \left\langle\Delta\tilde{\mathbf{r}}_i^B\Delta\tilde{\mathbf{r}}_i^B\right\rangle = 2\mathbf{I}\Delta\tilde{t}, \quad (9)$$

$$\left\langle\Delta\tilde{\mathbf{\Omega}}_i^B\right\rangle = 0, \quad \left\langle\Delta\tilde{\mathbf{\Omega}}_i^B\Delta\tilde{\mathbf{\Omega}}_i^B\right\rangle = \frac{3}{2}\mathbf{I}\Delta\tilde{t}. \quad (10)$$

The rotation of the particle in three dimensions presents some difficulties in tracking, therefore the quaternion parameters e_0, e_1, e_2, and e_3 are used to obtain the proper orientation.[31] Quaternion parameters can be defined in terms of Euler angles[32] and satisfy the relation:

$$e_0^2 + e_1^2 + e_2^2 + e_3^2 = 1. \quad (11)$$

In our code, three quaternion parameters are initialized randomly between -1 and 1, and the fourth by $e_0' = 1 - e_1'^2 - e_2'^2 - e_3'^2$. To satisfy the relation of the Euler angles, we use $(\mathbf{e}(0) = \mathbf{e}'(0)/|\mathbf{e}'(0)|)$, where $(\mathbf{e}'(0) = [e_0' \quad e_1' \quad e_2' \quad e_3'])$ and $(\mathbf{e}(0) =$

$[e_0 \quad e_1 \quad e_2 \quad e_3])$. The rotation matrix $\mathbf{A}(0)$ at initial time for all particles, can be written in terms of quaternion parameters:

$$\mathbf{A}(0) = \begin{pmatrix} e_0^2 + e_1^2 - e_2^2 - e_3^2 & 2(e_1 e_2 + e_0 e_3) & 2(e_1 e_3 - e_0 e_2) \\ 2(e_1 e_2 - e_0 e_3) & e_0^2 - e_1^2 + e_2^2 - e_3^2 & 2(e_2 e_3 + e_0 e_1) \\ 2(e_1 e_3 + e_0 e_2) & 2(e_2 e_3 - e_0 e_1) & e_0^2 - e_1^2 - e_2^2 + e_3^2 \end{pmatrix}. \quad (12)$$

Rigid body orientation vector $\mathbf{v}_{RB}'$, dipole orientation vector $\mathbf{v}_d'$ and shifted dipole vector $\mathbf{v}_s'$ are expressed in the mobile coordinate system, which are constant for all particles. Vectors $\mathbf{v}_{RB}$, $\mathbf{v}_d$ and $\mathbf{v}_s$ are expressed in the in inertial coordinate system, which is different for each particle:

$$\mathbf{v}_i = \mathbf{A}_i^T(\tilde{t})\cdot\mathbf{v}', \quad (13)$$

$$\mathbf{v}_i = \begin{pmatrix} x_i \\ y_i \\ z_i \end{pmatrix}; \quad \mathbf{v}_{RB}' = \begin{pmatrix} 0 \\ 0 \\ 1 \end{pmatrix}; \quad \mathbf{v}_d' = \begin{pmatrix} 0 \\ 0 \\ 1 \end{pmatrix}; \quad \mathbf{v}_s' = \begin{pmatrix} 0 \\ 0 \\ s \end{pmatrix},$$

where $\mathbf{A}_i^T(\tilde{t})$ is the transposed matrix of $\mathbf{A}_i(\tilde{t})$ and the same for all particles at t = 0. The time evolution of quaternion parameters is related to the total torque of the particle in the mobile rigid body system $(\tilde{\mathbf{T}}_i'(\tilde{t}) = \mathbf{A}_i(\tilde{t})\cdot\tilde{\mathbf{T}}_i(\tilde{t}))$ and the Brownian displacement vectors for the particles $\Delta\tilde{\mathbf{r}}_i^B(\tilde{t})$.

$$\boldsymbol{\omega}_i(\tilde{t}) = \left(\frac{3}{4}\Delta\tilde{t}\right)\tilde{\mathbf{T}}_i'(\tilde{t}) + \left(\frac{3}{2}\Delta\tilde{t}\right)^{1/2}\Delta\tilde{\mathbf{r}}_i^B(\tilde{t}), \quad (14)$$

$$\Delta\mathbf{e}_i(\tilde{t}) = \frac{1}{2}\begin{pmatrix} -e_1 & -e_2 & -e_3 \\ e_0 & -e_3 & e_2 \\ e_3 & e_0 & -e_1 \\ -e_2 & e_1 & -e_0 \end{pmatrix}\cdot\begin{pmatrix} \omega_{i1}(\tilde{t}) \\ \omega_{i2}(\tilde{t}) \\ \omega_{i3}(\tilde{t}) \end{pmatrix}, \quad (15)$$

$$\mathbf{e}(\tilde{t}+\Delta\tilde{t}) = \frac{\mathbf{e}(\tilde{t}) + \Delta\mathbf{e}(\tilde{t})}{|\mathbf{e}(\tilde{t}) + \Delta\mathbf{e}(\tilde{t})|}. \quad (16)$$

2.3 Simulated Parameters

Magnetic Janus colloids are analyzed with two non-constant control parameters, the dipolar shift s that regulates the anisotropic magnetic property of the magnetic Janus particles, and the dipolar coupling constant λ that controls the strength of the magnetic particle-particle interactions relative to the Brownian forces acting in the system, i.e.:

$$\lambda = \frac{\mu_0 m^2}{4\pi a^3 kT}. \quad (17)$$

The value of λ allows the determination of two regimes for the simulations, one that is dominated by the Brownian effect (low λ regime) and the other that is dominated by particle-particle magnetic interactions (high λ regime). In order to define where the system changes from low to high λ regime, $\lambda = 10$ to 90 were analyzed. This range is chosen because for $\lambda < 10$ the magnetic effect is not appreciable and the system is dominated by Brownian interactions, and for $\lambda > 90$ the magnetic interactions are very

strong generating over aggregation and does not allow the study of the dynamics of aggregation. Values of $s = 0$ to 0.8 have been analyzed, where $s = 0$ is a generic case of the DHS model that was used as control. The maximum radial shift achievable in the simulations is $s = 0.8$. For $s > 0.8$, the time step ($\Delta \tilde{t} = \Delta(t/\tau_D)$) required for numerical stability causes an unreasonable computational cost because of the proximity of the magnetic dipole to the surface. For $s \leq 0.7$, $\lambda_R = 2000$, $\delta/a = 0.01$ and $\Delta \tilde{t} = 10^{-4}$ are used. In contrast, for $s > 0.7$, a λ_R in the range from 2000 to 10000 is needed to increase the repulsive force, a δ/a of 0.01 to 0.10 is required to allow the repulsive force to act over a greater distance, and $\Delta \tilde{t}$ is set to 10^{-6} to address numerical instabilities problems. In order to obtain adequate statistics, five repetitions of each system are performed.

All simulations were performed with a surface fraction $\phi_s = 0.01$ —diluted system. At this surface fraction the long-range hydrodynamic and magnetic dipole-dipole interactions are not considered because their contributions are negligible on the structures and dynamics of aggregation.[33–37] Clearly, at higher surface fractions other numerical strategies, such as the Ewald summation method, must be implemented in order to quantify these long-range interactions.[36,38,39] The number of particles N is chosen to obtain a statistically representative system. HLR simulations are performed using $N = 1000$, and LLR simulations are performed using $N = 150$. The difference in the number of particles between HLR and LLR is due to the nature of the clusters in LLR (short lived clusters, with Brownian effect, predominates in the system). The clusters in LLR do not grow over time, by this, a large number of particles is not required to have statistically representative results. Additionally, the simulation has periodic boundary conditions, with a box length of $L = f(\phi_s, N)$. Particle i interacts with particle j if $r_{ij} \leq L/2$. The results are box size and time step independent.

2.4 Cluster Properties

Particle association with a cluster is determined by the bounding factor. The bounding factor is an dimensionless parameter that determines if two particles are in the same cluster, i.e., if the ratio of the distance between the center of mass of the particles and twice the radius—minimum possible distance between centers of mass—is less than the bounding factor, the particles are in the same cluster. To avoid erroneous quantification, based on statistical criteria, the value of the bounding factor that best determines the population of a cluster is 1.2.[18,40,41]

The dynamic process of aggregation is divided into nucleation and growth regimes, which are clearly identified using the difference between the total number of clusters (N_c) and the number of singlets (N_s), i.e., clusters with only one particle, as it scales with the number of particles N_P. The nucleation factor n_c is calculated as follows:

$$n_c = \frac{N_c - N_s}{N_p}, \tag{18}$$

also, using the number of particles per cluster $N_{c,p}$, the weighted

average mean cluster size is calculate as follows:

$$\langle N_c \rangle = \left\langle \frac{\sum_{p=1}^{N_c} (N_{c,p})^2}{\sum_{p=1}^{N_c} N_{c,p}} \right\rangle. \tag{19}$$

Finally, in order to characterize the cluster structures, the orientation distribution function of the particles is used, i.e., the probability of orientation distribution $P(\mathbf{m}_i \cdot \mathbf{m}_j)$ vs. the orientation distribution $\mathbf{m}_i \cdot \mathbf{m}_j$ considering two particles that are in the interaction range of each other. It should be noted that the number of neighbors that a particle will have is determined by the dipolar orientation at the minimum energy configuration. Figure S2 in the Supporting Information displays the minimum energy behavior for different configurations of pairs of particles, where a clear differentiation between three marked behaviors can be seen. Additionally, the orientation distribution function is constructed considering pairs of neighbor particles, i.e., each pair of particles with $r_{ij} \leq 1.2(2a)$. If there are more than two particles in contact simultaneously, each possible pair will be considered individually.

3 Results

3.1 Building Blocks

The dynamic evolution of the studied system presents marked structural variations for different values of λ and s. In order to characterize these structures, it is imperative to focus on the basic structures that serve as nuclei in the growth of final clusters. Fig. 2 shows the precursor clusters, i.e., aggregates with the critical nucleus size, that by their configuration of orientation and size are the building blocks (BBs) from which long-lived clusters are formed for each cluster phase.

When two or more magnetic particles interact with each other, generating attractive or repulsive forces according to the polarity (direction) of the dipoles, the particles will rotate to try to align their dipoles to reach the minimum energy configuration. Observation of the different structures reveals that the minimum energy configuration depends on the dipolar shift, i.e., the distance between the dipolar centers of different particles and the arrangement of the particles in contact changes to reach minimum energy configuration. In the insets of Fig. 2 the geometric configuration of the dipoles is shown. These orientations and the particle geometry limitations are the generators of the building blocks.

We can delineate two regimes of λ, the low λ regime (LLR) ($\lambda < 20$), and the high λ regime (HLR) ($\lambda \geq 20$). In LLR (Fig. 2a-f) no aggregation is observed at long times despite the presence of BBs similar to those observed in the HLR. Formation of long-lived cluster is inhibited by the Brownian effect that predominates in the system. In contrast, in HLR (Fig. 2g-u), a nucleation and growth regime are observed.

The LLR regime can be separated into two distinct aggregation behaviors. The first for $s < 0.7$ (Fig. 2a-c) shows growth based on cluster-cluster aggregation of the BBs and breakdown of clusters (including BB) by the Brownian effect resulting in a gas-like system. The behavior observed occurs because the magnetic potential given by the dipole in the hard sphere is contained within the particles and is small compared to the Brownian effect thereby
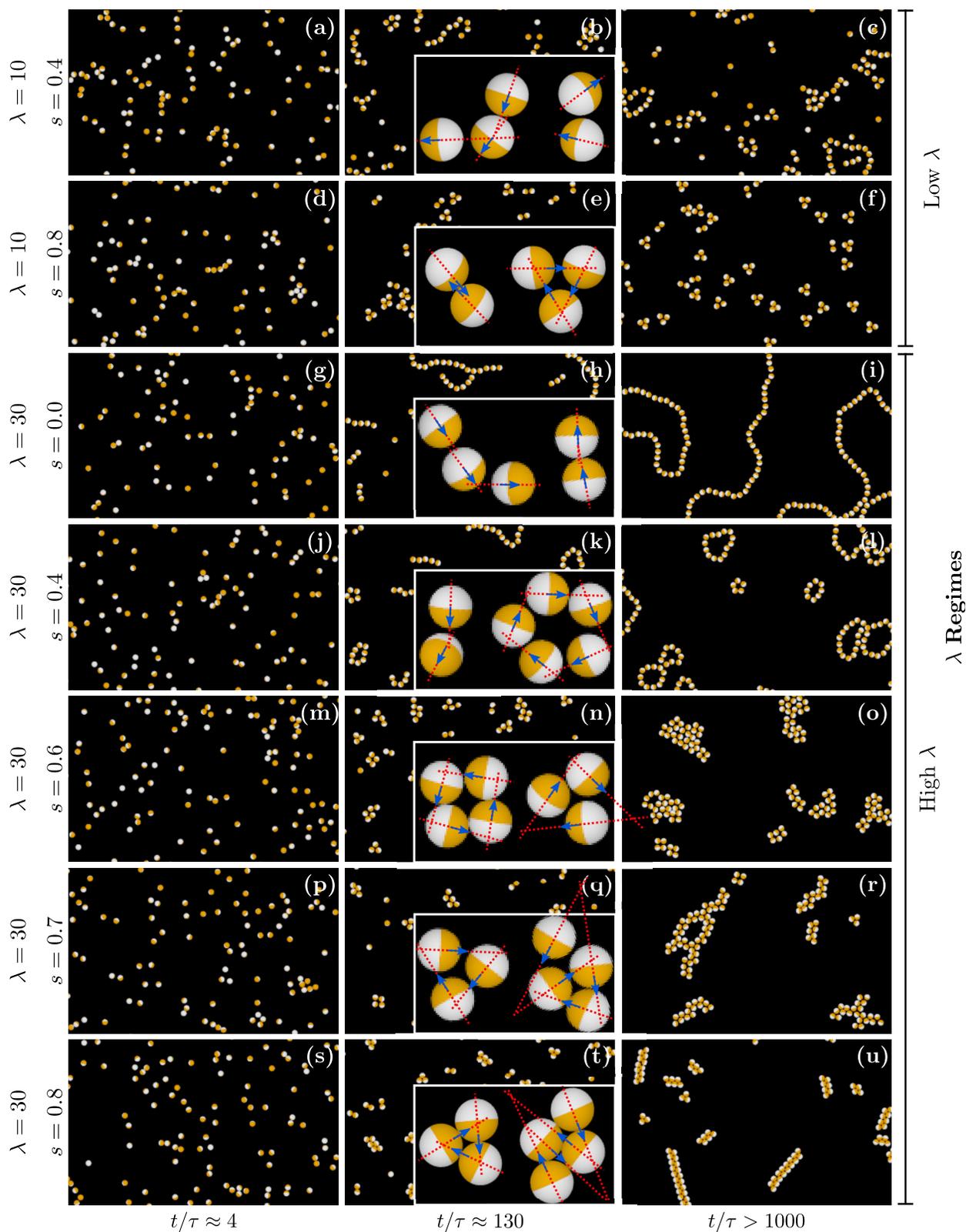
Fig. 2 Simulation renderings of systems of $\lambda = 10$ (LLR) and $\lambda = 30$ (HLR) at $s = 0$, 0.3, 0.5, 0.7, and 0.8 as a function of time. Panels (a), (d), (g), (j), (m), (p), and (s) show overviews of the initial clusters formed. Panels (b), (e), (h), (k), (n), (q), and (t) show the building blocks (critical nucleus size) that are the precursors of the long-lived clusters. Panels (c), (f), (i), (l), (o), (r), and (u) show the long-lived clusters with each system's characteristic clusters. Shifted magnetic dipoles are applied to the orange regions. Videos of the simulations are included in the Supporting Information.

not exerting enough attraction to maintain the structural stability of clusters.

The opposite happens when $s \geq 0.7$ (Fig. 2d-f). Although the magnetic potential does not have enough strength to generate cluster-cluster aggregation, the magnetic dipole is so close to the surface that the magnetic interaction is not restricted within the hard sphere, which gives rise to a short-range aggregation and the formation of permanent triplet clusters. The system saturates at triplets, owing to the fact that it represents the minimum energy structure for this value of s.[?] As a result, the Brownian effect is not strong enough to break these BBs but generates enough resistance to prevent the growth of larger clusters.

In LLR, the BBs have different structures that impact the aggregation at longer times. At $s < 0.7$, single-chains of doublets occur with head-to-tail aggregation. These single-chain clusters grow linearly, and according to the dynamics they form rings and loops that end up breaking at longer times. For the phase of $s \geq 0.7$ the BBs are triplets that do not show long-time cluster-cluster aggregation.

For HLR (Fig. 2g-u), the dynamic behavior is dominated by the magnetic potential, i.e., the BBs are formed permanently and in their evolution over time they form stable clusters. For $s \leq 0.4$ the BBs are doublets (Fig. 2h,k) that exhibit a head-to-tail aggregation configuration. A coexistence between single-chains and rings occurs for $s \leq 0.3$ (Fig. 2i) and structured loops form at $s > 0.3$ (Fig. 2l). Interestingly, these structures despite having the same BBs represent differentiations in the dynamic growth and tend to aggregate into clusters that are each time more compact and shorter—a tendency that increases with s.

For $s > 0.4$ and $s < 0.65$, the BBs present are triplets and quadruplets (rectangular arrangement) as shown in Fig. 2n. The structures grow bi-directionally, i.e., the size they can reach depends only on how many particular elements are present in the system with the tendency to form a single final cluster if the system is given enough time (Fig. 2o). The coexistence of these two types of BBs will be analyzed later in the dynamic growth section.

For $s \geq 0.65$ and $s \leq 0.75$ the BBs are triplets (Fig. 2q). The triplets will aggregate into structures that will continue to grow whenever they find particles in the system. Owing to their amorphous shape, they have the peculiarity of orienting their aggregation that allows for the formation of hollow zones (Fig. 2r).

The last phase analyzed is $s \leq 0.8$, the BBs are quadruplets (parallelogram arrangement) as shown in Fig. 2t. The clusters formed exhibit an oriented growth with a double-chain structure. Here, the magnetic dipole is very closed to the surface of the particle, which causes a marked anisotropy in the particle, i.e., it generates a magnetic zone in the central part of the cluster and a non-magnetic zone in the lateral regions. This sharp demarcation of magnetic and non-magnetic parts prevents other particles to be added to the non-magnetic sides of the cluster resulting in a double-chain configuration that grows linearly without loops in its structure (Fig. 2u). In addition, the magnetic potential is so strong that the time needed to observe the structures is shorter than that for other phases, because $r_{d_{ij}}$ is shorter than in the other systems and the magnetic force is greater.

3.2 Dynamic Growth

The dynamic process in the systems studied can be expressed by a two continuous processes, i.e., nucleation-growth, as shown in Fig. 3a. At an initial moment the system is only composed of singlets that move due to the Brownian motion and the forces that interact in them (gas-like system), the nucleation process determines the conformation of the BBs by particle-particle aggregation, and the growth process, in which the BBs join to form clusters of greater size by cluster-cluster aggregation. The two processes are quantified using the nucleation factor n_c. Plotting the n_c value as a function of time allows us to distinguish the appearance of the BBs and then observe the growth of the clusters. The first step in the dynamic process is the nucleation of the BBs. Nucleation happens from $t/\tau_D = 0$ in a particle-particle aggregation process characterized by an increase in the number of non-individual clusters and decrease of singlets in the system, i.e., formation of BBs and small clusters, until a critical time at which the difference between the number of non-individual clusters and singlets reaches a maximum. At the critical time, the BBs begin to aggregate with each other in a cluster-cluster aggregation process where the number of non-individual clusters decreases, while the number of particles per cluster increases, i.e., cluster growth occurs.

The expected nucleation and growth process behavior for LLR is a permanent nucleation process and truncated growth, because, in this system, large, long-lived clusters do not have the capacity to maintain themselves over time. As is apparent from Fig. 3a. For LLR the growth process does not occur, staying in a continuous nucleation process. The perpetuity of the nucleation process for $s < 0.7$ is mainly due to the disintegration of the clusters, i.e., the growth of the system by the magnetic interaction competes with the breakdown of the clusters due Brownian effect that predominates in the system, so the system remains permanently in a system of singlets and short-lived-clusters. In this competition, even the BBs are broken and reformed over time, which makes cluster-cluster aggregation that characterizes the growth process impossible.

In the case of $s \geq 0.7$ neither cluster breakdown nor growth are observed. The BBs have enough stability so that the Brownian effect does not break the BBs because the magnetic potential is mostly concentrated in the core of the cluster, increasing its structural stability but at the same time weakening its interaction with other clusters. The triplet BBs have an anisotropic distribution of magnetic interactions with a strongly magnetic part in their core and a non-magnetic part at the exterior leading to a weakening of long-range magnetic interactions and stabilization of the triplet BBs in the system over time.

The behavior of the nucleation and growth for HLR shows clear evidence for growth at longer times. For all s values, a pronounced maximum in n_c is observed (Fig. 3a) caused by the decrease of the number of clusters in the system and a notable tendency to form larger clusters with growth limited only by the number of particles in the system. The most outstanding observation is the rate at which the decrease of n_c occurs as a function of s, where for $s \leq 0.3$ the rate of decrease is very similar while for
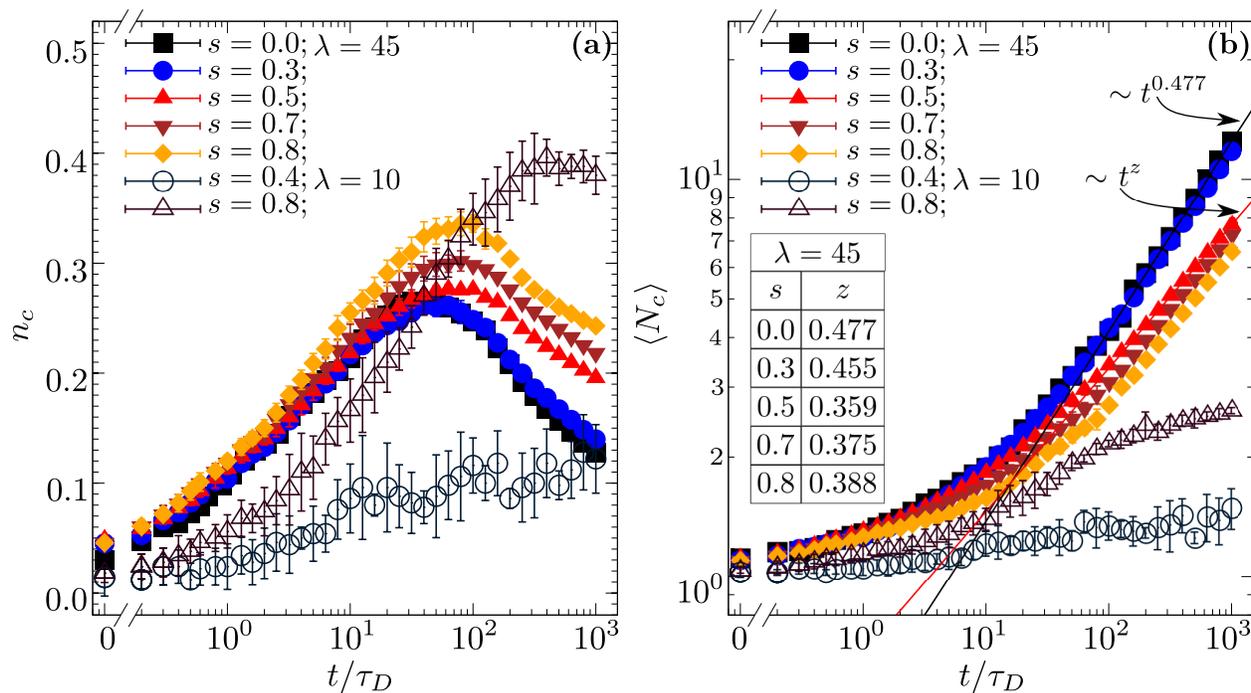
Fig. 3 Time effect on the aggregation behavior for both λ regimes. Panel (a) shows dynamic aggregation in two steps—nucleation and growth—as a function of time for LLR and HLR. Panel (b) shows weighted average mean cluster size $\langle N_c \rangle$ for LLR and HLR, as a function of time for various s, additionally, the power law behavior at long-time is represented by continuous lines. Filled symbols correspond to HLR systems, while open symbols correspond to LLR systems.

$s > 0.35$ the rate of decrease is lower.

Analysis of the weighted average mean cluster size $\langle N_c \rangle$ provides insight into the growth process. In Fig. 3b, we can see that for LLR $\langle N_c \rangle$ values saturate at small numbers of particles per cluster, where the average for $s < 0.7$ is between one and two particles per cluster (due to the cyclical breakdown of the clusters) and for $s \geq 0.7$ stabilizes at three in good agreement with the triplet BBs observed at long times.

In contrast, for HLR we observe power law behavior of the form $\langle N_c \rangle \sim t^z$, where the z exponent describes the growth rate. In the Figure S1 in the Supporting Information we can observe the power law for different values of s at HRL. The first trend observed is a slow deceleration of the growth rate for $s \leq 0.3$ from $z = 0.477$ to 0.359. Next, an abrupt acceleration in growth rate between $s = 0.35$ and $s = 0.5$ is observed from $z = 0.359$ to 0.455. Between $s = 0.55$ and $s = 0.7$ the growth rate decreases again to $z = 0.375$, whereas acceleration of growth rate is observed between $s = 0.75$ and $s = 0.8$. Note, the acceleration is much slower compared to the acceleration observed between $s = 0.35$ and $s = 0.5$. These four zones in which the growth rate varies provide further insight into different aggregation modes.

This change in the power law behavior occurs, because, while s increases, the area with the highest magnetic charge in the particle is reduced, thus at high s the area of magnetic interaction is practically reduced to the contact surface between particles and decreasing the maximum number of particles that can be stable at a minimum energy configuration in the same cluster. The limits of the different aggregation behaviors are determined by these distances, where the configurations are determined by the geom-

etry of the particles and how this alters the structure of the cluster to find the minimum energy configuration. Especially for LLR where the magnetic interaction is overcome by the Brownian effect, in Fig. 3a for $s \geq 0.65$ the minimum energy configuration for three particles is obtained by an equilateral triangle dipole configuration (Fig. 2e), this configuration is due to the proximity from the center of the magnetic dipole to the surface of the particle. It manages to overcome the Brownian effect and allows these triplets to be stable over time, but due to the low magnitude of the dipoles, they do not have enough energy to attract other triplets and grow.

3.3 Long-time Structures and Cluster Phases

Analyzing the different aggregation behaviors occurring at long times as a function of s, clusters can be grouped into different phases. In our assignments, we consider an average of the clusters observed in the final 20% of the simulation to predict the behavior and order of clusters at long times.

For LLR, it is apparent from Fig. 4a,b that the populations of clusters do not show growth in good agreement with our findings during analysis of the dynamic processes. The populations for HLR are plotted as a function of the characteristic times $(t/\tau_D = 10^0, 10^1, 10^2, 10^3)$ during which the populations show growth but with variations in the growth rate. In Fig. 4 g,j, we observe that for the cluster phase $0 \leq s \leq 0.3$ the populations present a tendency very similar to those observed by Vicsek[42] with a logarithmic decrease in the amount of clusters according to the increase in the number of particles per cluster, which indicates that the aggregation process is identical to those observed
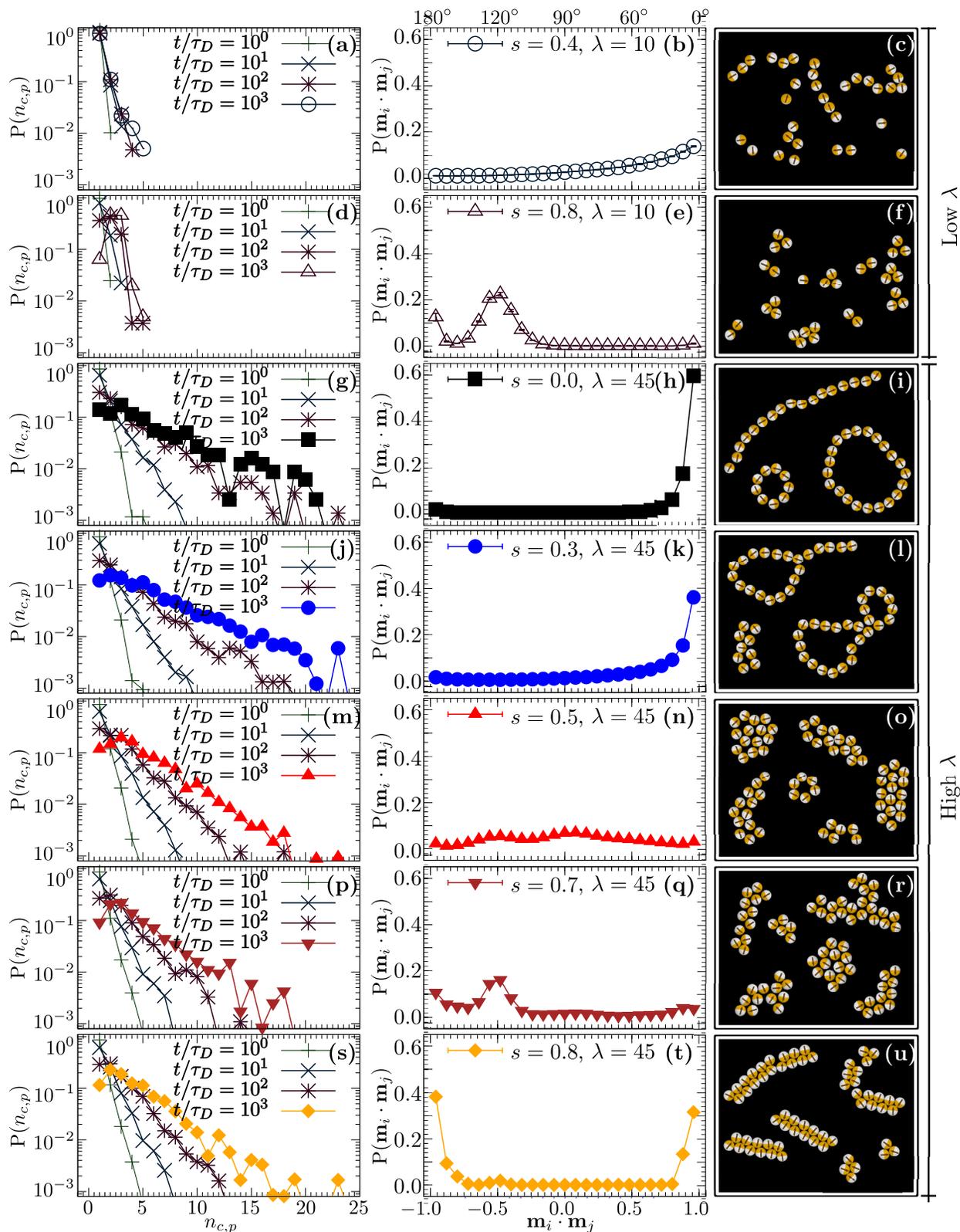
Fig. 4 Effect of dipolar shift on the cluster size distribution $P(N_{c,p})$ and orientational distribution function $P(\mathbf{m}_i \cdot \mathbf{m}_j)$ in relation to the different cluster phases. Panels (a), (d), (g), (j), (m), (p), and (s) show cluster size distribution for four different times. Panels (b), (e), (h), (k), (n), (q), and (t) show the particle orientation distribution functions for each phase's characteristic clusters. Panels (c), (f), (i), (l), (o), (r), and (u) contain the characteristic clusters for each phases.

in magnetic particles with centered dipoles, whose aggregation behavior has been studied for a long time and can be found in the literature.[43,44]

In the second HLR phase, Fig. 4m, with intermediate dipolar shifts of $0.35 \leq s \leq 0.6$, a distribution in the population is observed that decreases up to a critical number of particles per cluster and then tends to conserve the same population for larger clusters. This behavior indicates an isolation of larger clusters in the system, i.e., the relative distance between larger clusters is so large that they do not experience magnetic attraction with each other and only grow by depletion of smaller clusters that are spread throughout the system in a region close to them resulting in isolated islands.

The cluster size distributions in the phase of $s \geq 0.65$ as shown in Fig. 4p,s exhibit population trends of growth and decline with an overall decreasing tendency. This behavior indicates a growth very similar to that observed for magnetic particles with centered dipoles but with a tendency to accumulate clusters of certain sizes or special configurations indicating that there is a necessary condition for the cluster-cluster aggregation, i.e., there is a preferred configuration for aggregation and when clusters are not found in this particular configuration they do not aggregate despite being close enough for aggregation until the required orientation is obtained. Such an aggregation depends not only on time but also on cluster configuration and location. Analysis of the configurations shown in Fig. 4r,u clearly shows that these clusters only grow in preferential directions resembling directed growth.

Using the information obtained for long times (average of the last 20%), we can obtain the predominant dipole orientation in the cluster. The orientation distribution provides the internal orientation of the dipoles in the cluster and provides insight into the properties of the aggregates yielding basic characteristics of the system such as cluster stability.

The interactions between nearest-neighbor particles are reflected in the dipolar orientations, this can be observed in the orientation distribution function. When s changes, the directions of the dipoles for the minimum energy configuration changes. Figure S2 in the Supporting Information shows this phenomenon, parallel orientation $(0°)$ is predominant for low shifts $(s \leq 0.35)$, a range of values $(60° − 120°)$ for medium shifts $(0.35 < s < 0.65)$, and two values $(120°$ and $180°)$ for high shifts $(s \geq 0.65)$. Thus, for each aggregation mode, there is a range of representative angles between dipoles, and these configurations also determine the structure of the building blocks.

In LLR, we observe two different behaviors, so we can distinguish two types of aggregates. For $s < 0.7$, Fig. 4b,c shows a distribution of the orientation of their structures preferably parallel $(\mathbf{m}_i \cdot \mathbf{m}_j = 1)$, but with a low probability of finding them in this orientation, which implies that most of the time they exist as singlets. Thus, this phase is assigned the name Short-Lived-Clusters (SLC) phase. Furthermore, for values of $s \geq 0.7$ (Fig. 4e,f) the orientation of the aggregates is predominantly at an angle of $\mathbf{m}_i \cdot \mathbf{m}_j = -0.5$. The angle is characteristic of equidistant triangles, but due to its low magnetic potential (see above), cluster growth never happens and the BBs are perpetuated as triplets, hence we name it the Triplets phase.

For HLR, five different aggregation behaviors are observed for $s < 0.3$, $0.3 \leq s < 0.55$, $0.55 \leq s < 0.65$, $0.65 \leq s \leq 0.75$ and $s > 0.75$.

In the $s < 0.3$ phase, Fig. 4h,i, the preferred orientation is parallel with a head-to-tail aggregation behavior. This phase is strongly resembling the aggregation behavior of magnetic particles with centered dipoles, whose growth is clearly in the form of infinitely long chains with their growth potential limited only by the number of particles. Thus, the phase is named Single-Chains phase.

For $0.3 \leq s < 0.55$, Fig. 4k,l, the preferred orientation is again parallel with head-to-tail aggregation, but unlike in the Single-Chains phase, additional aggregation in directions with acute angles is observed resulting in formation of short rings and chain-based amorphous clusters. Growth is again only limited by the number of particles, and although there are closed rings, when a particle approaches these clusters, they open and accept new particles. Summarizing these characteristics, the phase is named Loop-like phase.

In the $0.55 \leq s < 0.65$ phase, see Fig. 4n,o, a distribution of aggregation preferences is observed. Three orientations with $\mathbf{m}_i \cdot \mathbf{m}_j = 0.5, 0, -0.5$ are observed, which allows an aggregation in the form of triangles and squares leading to non-linear, multidirectional growth. A maximum number of particles in the smallest area yields compact clusters with very little empty space, where a particle often has six neighbors. In addition, formation of isolated islands was observed therefore giving it the name Island-like phase.

For $0.65 \leq s \leq 0.75$, Fig. 4q,r, the system is clearly within the directed aggregation zone, whose preferred orientation is $\mathbf{m}_i \cdot \mathbf{m}_j = -0.5$. This orientation corresponds to triangular clusters, but with an obtuse angle that allows a growth similar to that observed in the Island-like phase. However, the obtuse angle preference in this phase impacts the configuration of the cluster, representing directed aggregation, with the possibility of ring, double-chain and amorphous forms, which has been termed Worm-like phase in the literature.[45]

In the $s > 0.75$ phase, Fig. 4t,u, the system is still in the directed aggregation zone, but with preferred orientations that are both antiparallel $(\mathbf{m}_i \cdot \mathbf{m}_j = -1)$ and parallel $(\mathbf{m}_i \cdot \mathbf{m}_j = 1)$. This orientational preference causes the clusters to be added in a linear fashion leading to chains with a highly magnetic center and non-magnetic rims. The resulting aggregation is exclusively by either head or tail forming a double linear chain. It can be seen that the orientation of preference for balance is the antiparallel one where the parallel orientation is generated as an outcome of the oriented growth of the double-chain, for which this phase is called Antiparallel-Double-Chain (ADC) phase.

In summary, two aggregation phases are found for LLR and delineated by s, while for HLR five phases are identified by varying s that show three aggregation modes, which are determined by analysis of the dynamic processes of nucleation and growth.

3.4 Aggregation Modes

We have observed that the cluster phases are within aggregation modes defined by the rate of aggregation and the population distribution. Using this information together with the orientation

function, we can define these modes more clearly and assign characteristics to them. It must be noted that according to λ of the system, the aggregation modes and the cluster phases fall between different values of s; however, despite the change in s, the behavior and characteristics of the aggregation modes are equal.
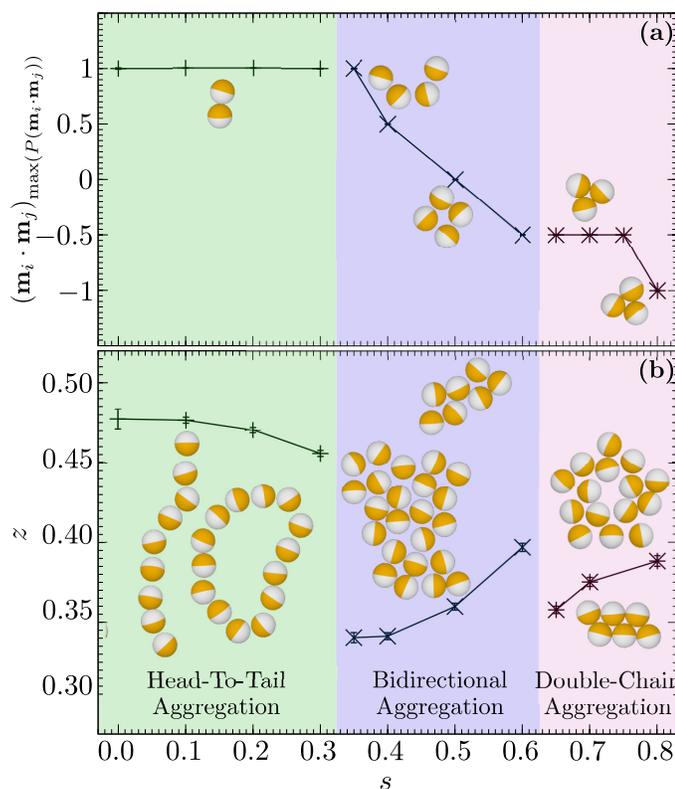

Fig. 5 Effect of dipolar shift at $\lambda = 45$ denoting three aggregation modes. Panel (a) shows the particle orientations of the maximum probability particle orientation as a function of s. Panel (b) shows the Power law exponent (z) as a function of s. Each aggregation mode is differentiated by a color: Head-to-Tail-Aggregation (green), Bidirectional-Aggregation (Blue), and Double-Chain-Aggregation (rose).

For $s = 0$ to 0.8 at $\lambda = 45$ (Fig. 5), the behavior of the orientations with maximum orientation probabilities ($\max(P(\mathbf{m}_i \cdot \mathbf{m}_j))$) and the power law exponent (z), show three different behaviors for the same values of s ($0 \leq s < 0.35$, $0.35 \leq s < 0.65$ and $s \geq 0.65$)).

We can see that the growth speed of the clusters is tied to the relative orientation between particles, i.e., the direction of growth of the clusters limits the growth speed. In addition to this observation, the orientation also presents three different opportunities for growth. The first one is head-to-tail aggregation in which the preferential orientation is parallel and shows identical growth behavior reported for magnetic particles with a centered dipole, i.e., growth along a chain with the capacity of attaching to other chains with ease regardless of the point of contact. Furthermore, the amorphous form of the loop-like aggregation would explain the slow deceleration of the growth rate toward larger s, since the closed forms of the chains trigger a process of depletion near each cluster as the area occupied and the number of particles per cluster decrease.

The first abrupt reduction in growth that occurs between $s = 0.3$ and $s = 0.35$ is ascribed to the range of possible aggregation orientations. Although the ability of the BBs to be triangles or squares that generates a bidirectional aggregation in the xy plane in which the particles move and can join the cluster in any direction should lead to an acceleration of the growth rate, a simultaneous reduction in the effective magnetic momentum generates isolated islands that depend solely on diffusion processes to be able to find each other and grow.

The slow acceleration of the growth speed in the bidirectional aggregation mode is due to the fact that it passes from triangles of acute angles that allow having six neighbors for each particle to square BBs that allow only four neighbors for each particle and then to triangular BBs but with an obtuse angle that generates a directionalization of the aggregation generating elongated and less compact islands. As a result, clusters with the same number of particles occupy a larger area of the system, which brings the clusters closer together allowing the effective radius of the magnetic momentum to attract other clusters more easily and in this way to slowly accelerate the growth speed.

The second abrupt deceleration in growth happens when the magnetic dipole is so close to the surface of the particle that the magnetic moment is more noticeable on the surface towards which it has moved. The more pronounced directionality of growth slows down growth, not as abruptly as in the $s = 0.3$ and $s = 0.35$ transition, but still significantly. Structures called worm-like are formed with a double-chain amorphous structure. Although the area they occupy is greater than the isolated islands of the intermediate region, having the magnetic dipole so close to the center of the clustering structure, forces the cluster-cluster aggregation process to be carried out in specific areas of its structure, which in turn generates the abrupt reduction in growth rate observed between $s = 0.6$ and $s = 0.65$. Then, the slow acceleration of the growth speed is again caused by the tendency to linearize the cluster to antiparallel and form double-chains increasing the cluster area and the closeness between clusters. When the full linearity of the double-chain is reached the growth speed tends to a horizontal asymptotic.

It is important to mention that these three aggregation modes are present only in HLR, because in LLR the relationship between the magnetic moment and the Brownian effect is not strong enough for it to result in growth.

The three aggregation modes depend intrinsically on the angle between dipoles of neighboring particles, since this orientation allows the aggregation that characterizes each mode.

The modes do not fall into the same s rage for varying values of λ. At HLR, the aggregation modes move to a lower value of s upon increasing λ. The change is not large but needs to be taken into account for future applications. The only aggregation mode that is permanent in s is the double-chain aggregation, which depends intrinsically on the proximity of the magnetic dipole to the surface of the particle, i.e., it does not depend directly on λ, which is a sufficient condition for HLR.

3.5 Structural "Phase" Diagram

The Janus particle system with radically shifted dipoles gives access to a large variety of possible configurations for clusters, which have their own characteristics of nucleation (BBs) and growth. Their rich behavior allows us to create a structural "phase" diagram based on the relation of λ and s as shown in Fig. 6a. The structural "phase" diagram is constructed with the two λ regimes and the three aggregation modes as criteria for its construction. Each has its own building block and a different distribution of orientations. The relation between the structural phases, λ regimes and the aggregation modes are shown in Table 1. Each point is the result of five simulations repeated at identical conditions with random initial particle and orientation distributions.

Table 1 Relation between Structural Phases, λ Regimens and Aggregation Modes at Radially shifted dipole systems:

Structural Phase	λ Regime	Aggregation Mode
SLC	LLR	Head-To-Tail
Triplets	LLR	Double-Chain
Single-Chain	HLR	Head-To-Tail
Loop-Like	HLR	Head-To-Tail
Special-Coexistence	HLR	Head-To-Tail/Bidirectional
Island-Like	HLR	Bidirectional
Worm-Like	HLR	Double-Chain
ADC	HLR	Double-Chain

The structural "phase" diagram limits depend of the dipole arrangement geometry of the building blocks, which will be grouped and ordered to reach a minimum energy. Fig. 6a shows displacement of these limits to the left at $s < 0.65$ with the increase of λ, this is due to the fact that the generated magnetic forces are physically capable of attracting the particles more easily to each other. On the other hand, at $s \geq 0.65$ due to the closeness of the center of the dipole to the surface of the particle, the building blocks are formed around the area of greatest magnetic load—near the surface of the interparticle contact, by this, the increase of λ does not influence on the structural "phase" diagram limits.

There are eight phases in the structural "phase" diagram, which are divided into two regimes dependent on λ. The first LLR phase happens for a situation where λ is high enough to overcome the Brownian effect in the colloidal medium, but at the same time is too low to maintain stable clusters over time. In this regime two phases occur dependent on s; (i) the SLC phase, which presents a cycle of nucleation and perpetual breaking with the average size of the cluster being less than or equal to two particles per cluster while formation of short chains and structures similar to small islands is observed for short periods of time and (ii) the Triplets phase, in which although the magnetic effect is not large enough to maintain a stable cluster, the nearness of the dipole to the surface allows the magnetic dipoles to be close enough to each other to maintain a stable triangular structure.

The second regime that dependents on λ is HLR. This regime has six phases, these phases are distinct in their aggregation orientation. The phase with the lowest s is the Single Chain phase. Immediately next to it is the Loop-like phase. Both phases have characteristics and properties very similar to magnetic particles with centered dipoles and exhibit a characteristic head-to-tail ag-

gregation. The main difference between these two phases is that the Loop-like phase has the ability to aggregate particles with acute angles that allows having small rings and loops with greater ease than in the Single-Chain phase where chains dominate.

For an s of intermediate size, a phenomenon occurs that alters the aggregation of the system, i.e., bidirectional aggregation is observed in the xy plane containing the particles. This aggregation generates compact isolated islands for which the area and the number of particles per cluster decreases as s increases causing the clusters to be less compact owing to the greater s and at the same time decrease their isolation.

For high values of s, there are two phases that are only dependent on s, that is, independent of the value of λ at HLR. They will always be found for the same range of s values, where $0.65 < s < 0.75$ leads to Worm-like and $s > 0.75$ to Antiparallel-Double-Chain (ADC) phases. These two phases together with the Triplets phase in LLR have as their main feature the nearness of the magnetic dipole to the surface of the particle.

This proximity of dipoles forces interaction through the magnetic surface, making the non-magnetic surface not stable for aggregation yielding clusters with magnetic properties localized in the center of the cluster thereby forcing the directionalization of cluster growth. In the Worm-like phase, the clusters are not linear because BBs can be added at obtuse angles, which generates amorphous clusters and can lead to the formation of double-chain-rings. In contrast, the ADC phase is completely linear, so all the clusters are geometrically equal to each other with the number of particles in each chain being the only difference.

In addition to these seven structural phases, a Special Coexistence phase occurs between Loops and Islands Fig. 6b, this phase occurs at $\lambda \geq 80$. The high value of the magnetic dipole in relation to the Brownian effect in this phase forces the aggregation of the particles in the xy plane, i.e., islands appear in the Loop-like phase. These islands are totally forced by the magnetic interaction and have the same structural characteristics as clusters belonging to the Island-like phase. Their structure is similar to islands joined by chains and loops. The phase is generated because the magnetic radius of each particle can affect not only the immediately neighboring particles, but also affects the non-adjacent particles. In this way an island is generated where the resulting magnetic potential is minimal although if the calculation is made only between immediate neighbors the magnetic potential is not at a minimum.

3.5.1 Hypothesis for $s > 0.7$ at $\lambda > 45$ and $s > 0.8$ at any λ

The following hypothesis arises as a result of computational limitations inherent to the Brownian dynamic simulation code. The values of the magnetic potential tend to infinity when $\mathbf{r}_{d_{ij}}$ tends to zero, which generates a computational error that cannot be corrected without sacrificing simulation time, which makes it unfeasible.

Using the magnetic potential (equation 3), the distance between dipoles ($\mathbf{r}_{d_{ij}}$) for the minimum energy is calculated for a pair of particles, if we make the equation independent of λ, then $\mathbf{r}_{d_{ij}}$ for the minimal energy is determined by s. The orientation between dipoles ($\mathbf{m}_i \cdot \mathbf{m}_j$) is determined by $\mathbf{r}_{d_{ij}}$. For $s > 0.75$ the min-
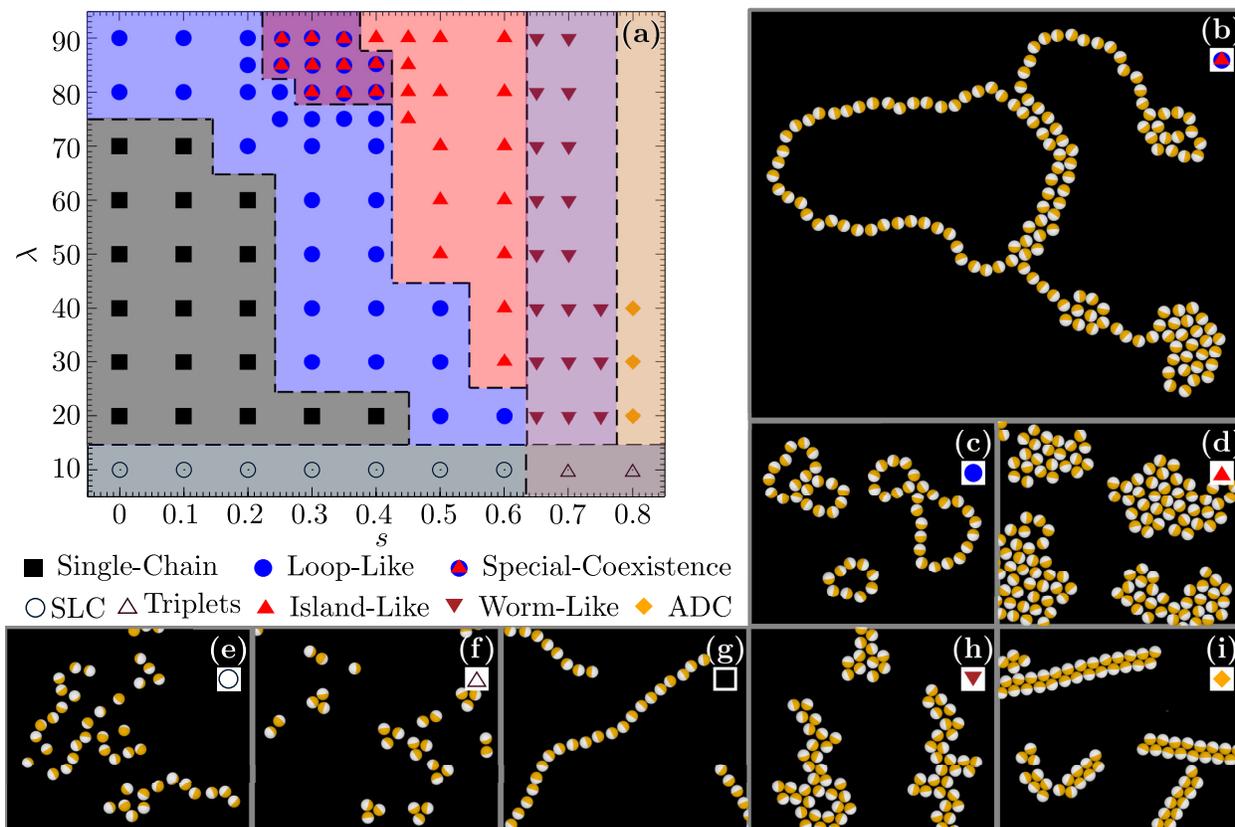
Fig. 6 Structural "Phase" diagram of cluster phases observed at long times. The radially shifted dipole shows different behavior of nucleation and growth as a function of λ and s. (a) Depicts a "phase" diagram of the cluster phases, (b) is a Special-Coexistence phase (Loops and Islands), (c) Loop-like phase, (d) Island-like phase, (e) SLC phase, (f) Triplets phase, (g) Single-Chains phase, (h) Worm-like phase, and (i) ADC phase

imum energy orientation calculated is antiparallel ($\mathbf{m_i} \cdot \mathbf{m_j} = -1$). From this observation, it can be inferred that the aggregation of all $s > 0.75$ is in the ADC phase. This conclusion is further supported by the fact that the phases grouped for $s \geq 0.65$ are independent of λ in HLR because their aggregation behavior is dependent on the closeness of the dipole to the surface of the particle and coincides with the results of Kantorovich.[20] From these arguments, the following is inferred: the cluster phase for $s > 0.7$ in $\lambda > 45$ and $s > 0.8$ in any λ can be set with the data of $s > 0.7$ in $\lambda > 20$ and $s \geq 0.8$ in any λ.

4 Conclusions

The dynamic study of magnetic Janus particles with radially shifted dipoles was carried out by Brownian dynamics simulations with different combinations of dipolar shift and magnetic interaction potentials. It is possible to distinguish between two regimes of aggregation that are defined by the existence (HLR) or absence (LLR) of cluster growth. In addition, there are three aggregation modes: Head-To-Tail (lower shift), Bidirectional (intermedium shift), and Double-Chain (high shift). Owing to the interplay between the two aggregation regimes and the three aggregation modes, we can find eight cluster phases: Two in LLR (SLC and Triplet phase) and six in HLR (Single-Chain, Loop-Like, Special-Coexistence, Island-Like, Worm-Like and ADC phase).

In the phases in HLR, it is observed that an increased dipolar shift generates clusters that are more and more compact. In addition, a decrease of the effective radius of the clusters from $s = 0$ (Single-Chain phase) to $s \approx 0.6$ (Island-Like phase) is observed followed by an increase of the effective radius as a result of the clusters tending towards elongated structures. Further, as the displacement of the dipole increases, the averaged mean cluster size decreases.

The interactions between nearest-neighbor particles are reflected in the dipolar orientations, this can be observed in the orientation distribution function. Parallel orientation (0°) is predominant in head-to-tail aggregation, a variation of the angle between 60° and 120° for bidirectional aggregation and 120° and antiparallel (180°) for double-chain aggregation. Thus for each aggregation mode, there is a range of representative angles between dipoles, and these configurations also determine the structure of the building blocks

The most significant parameter affecting the rate of cluster growth is λ—the growth rate increases as λ increases—but not significantly affecting the structures of the clusters or their dynamic process; but, for $\lambda \geq 80$ an over-averaging effect occurs due to the high magnetic potential, which generates a Special-Coexistence phase where both Loop-Like and Island-Like clusters coexist between $s = 0.3$ and $s = 0.4$.

The diversity of structures that can be achieved with this type of anisotropy in magnetic colloids, allows us to develop materials

with predictable characteristics. Island-like structures have the ability to form compact materials that allows the construction of monolayer magnetic colloids membranes, e.g. membrane of capsules for drug delivery where can direct the capsule through an external magnetic field with which to break the capsule when is necessary. ADC structures allow the construction of very long materials of very small thickness, in addition to growing as columns functioning perfectly as a support structure for larger structures. Likewise, the other types of structures allow a great diversity in the applications that can be used.

Conflicts of interest

There are no conflicts to declare.

Acknowledgments

References

1 R. B. Frankel, D. A. Bazylinski, M. S. Johnson and B. L. Taylor, *Biophys. J.*, 1997, **73**, 994–1000.

2 B. Moskowitz, R. B. Frankel, P. Flanders, R. Blakemore and B. B. Schwartz, *J. Magn. Magn. Mater.*, 1988, **73**, 273–288.

3 S.-J. Park, S. Kim, S. Lee, Z. G. Khim, K. Char and T. Hyeon, *J. Am. Chem. Soc.*, 2000, **122**, 8581–8582.

4 Y. Ichiyanagi, S. Moritake, S. Taira and M. Setou, *J. Magn. Magn. Mater.*, 2007, **310**, 2877–2879.

5 K. Mahmoudi and C. G. Hadjipanayis, *Front. Chem.*, 2014, **2**, 109.

6 V. V. Mody, A. Cox, S. Shah, A. Singh, W. Bevins and H. Parihar, *Appl. Nanosci.*, 2014, **4**, 385–392.

7 S. Campuzano, M. Gamella, V. Serafín, M. Pedrero, P. Yáñez-Sedeño and J. M. Pingarrón, *Magnetochemistry*, 2019, **5**, 47.

8 J. Yan, S. C. Bae and S. Granick, *Adv. Mater.*, 2015, **27**, 874–879.

9 P. Tierno, *Phys. Chem. Chem. Phys.*, 2014, **16**, 23515–23528.

10 Z. Jalilvand, A. B. Pawar and I. Kretzschmar, *Langmuir*, 2018, **34**, 15593–15599.

11 E. Bianchi, A. Z. Panagiotopoulos and A. Nikoubashman, *Soft Matter*, 2015, **11**, 3767–3771.

12 S. Gangwal, O. J. Cayre and O. D. Velev, *Langmuir*, 2008, **24**, 13312–13320.

13 J. Weis and D. Levesque, *Phys. Rev. Lett.*, 1993, **71**, 2729.

14 D. Levesque and J. Weis, *Phys. Rev. E*, 1994, **49**, 5131.

15 P. J. Camp, J. Shelley and G. Patey, *Phys. Rev. Lett.*, 2000, **84**, 115.

16 T. Prokopyeva, V. Danilov, A. Dobroserdova, S. Kantorovich and C. Holm, *J. Magn. Magn. Mater.*, 2011, **323**, 1298–1301.

17 A. B. Yener and S. H. Klapp, *Soft Matter*, 2016, **12**, 2066–2075.

18 G. I. Vega-Bellido, R. A. DeLaCruz-Araujo, I. Kretzschmar and U. M. Córdova-Figueroa, *Soft Matter*, 2019, **15**, 4078–4086.

19 L. Baraban, D. Makarov, M. Albrecht, N. Rivier, P. Leiderer and A. Erbe, *Phys. Rev. E*, 2008, **77**, 031407.

20 S. Kantorovich, R. Weeber, J. J. Cerda and C. Holm, *Soft Matter*, 2011, **7**, 5217–5227.

21 J. G. Donaldson, E. S. Pyanzina, E. V. Novak and S. S. Kantorovich, *J. Magn. Magn. Mater.*, 2015, **383**, 267–271.

22 D. Ermak, *Rapport d'activité scientifique du CECAM*, 1976, **1**, 66–81.

23 D. R. Foss and J. F. Brady, *J. Rheol.*, 2000, **44**, 629–651.

24 I. C. Carpen and J. F. Brady, *J. Rheol.*, 2005, **49**, 1483–1502.

25 A. Ruditskiy, B. Ren and I. Kretzschmar, *Soft Matter*, 2013, **9**, 9174–9181.

26 B. Ren and I. Kretzschmar, *Langmuir*, 2013, **29**, 14779–14786.

27 D. L. Ermak and H. Buckholz, *J. Comput. Phys.*, 1980, **35**, 169–182.

28 A. Satoh, *Introduction to molecular microsimulation of colloidal dispersions*, Elsevier, Amsterdam, 2003, vol. 17, pp. 127–152.

29 T. McIntosh, A. Magid and S. Simon, *Biochemistry-US*, 1987, **26**, 7325–7332.

30 B. Akpinar, L. A. Fielding, V. J. Cunningham, Y. Ning, O. O. Mykhaylyk, P. W. Fowler and S. P. Armes, *Macromolecules*, 2016, **49**, 5160–5171.

31 D. J. Evans, *Mol. Phys.*, 1977, **34**, 317–325.

32 H. Goldstein, C. Poole and J. Safko, *Classical Mechanics*, Addison Wesley, Reading, MA, 3rd edn, 2001, pp. 134–183.

33 S. H. Klapp, *Curr. Opin. Colloid In.*, 2016, **21**, 76–85.

34 M. Klinkigt, R. Weeber, S. Kantorovich and C. Holm, *Soft Matter*, 2013, **9**, 3535–3546.

35 E. V. Novak, E. S. Pyanzina and S. S. Kantorovich, *J. Phys.-Condens. Mat.*, 2015, **27**, 234102.

36 R. Gontijo and F. Cunha, *Phys. Fluids*, 2017, **29**, 062004.

37 A. Tomilov, A. Videcoq, M. Cerbelaud, M. A. Piechowiak, T. Chartier, T. Ala-Nissila, D. Bochicchio and R. Ferrando, *J. Phys. Chem. B*, 2013, **117**, 14509–14517.

38 M. Allen and D. Tildesley, *New York: Oxford*, 1989, **385**, year.

39 P. P. Ewald, *Ann. Phys.*, 1921, **369**, 253.

40 T. Edvinsson, P. J. Råsmark and C. Elvingson, *Mol. Simulat.*, 1999, **23**, 169–190.

41 F. G. Pierce, *Doctoral dissertation*, Kansas State University, 2007.

42 T. Vicsek and F. Family, *Phys. Rev. Lett.*, 1984, **52**, 1669.

43 K. Butter, P. Bomans, P. Frederik, G. Vroege and A. Philipse, *Nat. Mater.*, 2003, **2**, 88.

44 V. S. Mendelev and A. O. Ivanov, *Phys. Rev. E*, 2004, **70**, 051502.

45 R. A. DeLaCruz-Araujo, D. J. Beltran-Villegas, R. G. Larson and U. M. Córdova-Figueroa, *Soft Matter*, 2016, **12**, 4071–4081.
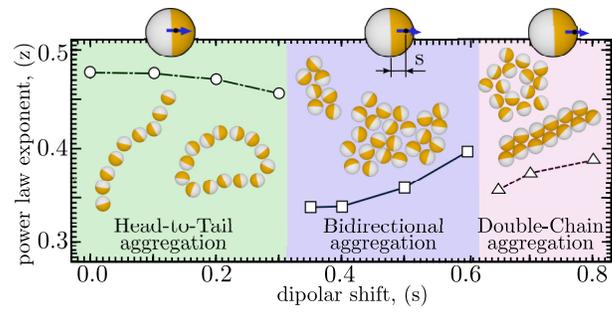
Graphical Abstract

The effect of dipolar shift on the rate of aggregation (t^z), the aggregation modes and structure of clusters is studied.